Mixed Valence of Bismuth in Hexagonal Chalcohalide Nanocrystals

Danila Quarta,$^{\circ}$ Stefano Toso,$^{\circ}$ Gabriele Saleh,* Rocco Caliandro,* Anna Moliterni, Andrea Griesi, Giorgio Divitini, Ivan Infante, Giuseppe Gigli, Cinzia Giannini, Liberato Manna, and Carlo Giansante*

ACCESS | Metrics & More | Article Recommendations | Supporting Information

ABSTRACT: We report the colloidal synthesis of bismuth chalcohalide nanocrystals, which adopt a hexagonal phase that we describe with the $Bi_{13}S_{18}X_2$ (in which X = Br and I) structure. Such a model structure displays columns of Bi atoms that form dimers of subvalent Bi (formally Bi_2^{4+}), which we here ascribe to Peierls-type distortions. We suggest that the Bi_2^{4+} dimers are at the origin of the anomalously low band gap of this material, with the lowest energy electronic transition showing analogies with an intervalence charge transfer. Our synthetic approach and insights into the structural and electronic features of the hexagonal bismuth chalcohalides are fundamental to sustain the rapidly increasing use of this class of (nano)materials for diverse applications, such as photocatalysis and thermoelectrics.

$Bi_{13}S_{18}X_2$ NCs — $Bi(II)-Bi(II)$ — IVCT
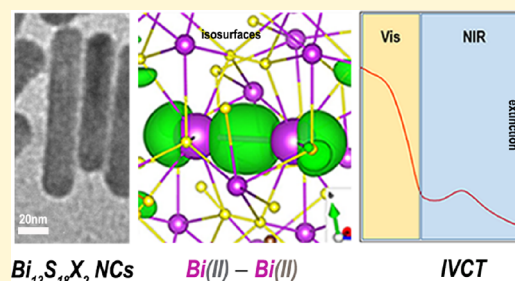
INTRODUCTION

Mixed valence in inorganic compounds refers to the presence of a metal cation in two different oxidation states showing interactions that may give rise to unusual optical, electrical, and magnetic properties.[1] The probably best-known example of a mixed valence compound, the ferric ferrocyanide salt called Prussian Blue, undergoes a ground state Fe(II)-to-Fe(III) charge transfer,[2] responsible for its peculiar color, and ferromagnetic exchange interactions, leading to magnetic ordering.[3] Mixed valence has also been related to other interesting phenomena, such as high-temperature super-conductivity[4] and colossal magnetoresistance.[5] To the aim of designing mixed valence compounds, main group metals featuring chemically stable low oxidation states may present ample opportunities, such as for the long-standing example of $Cs_4Sb(III)Sb(V)Cl_{12}$ and its dark color, unexpected for alkali pnictogen chloride salts.[6] The material size may also affect the properties of mixed valence inorganic compounds,[7,8] although they have seldom been investigated at the nanoscale despite offering an intrinsically high surface-to-volume ratio,[9] which may be exploited for photocatalytic purposes,[10] and the possibility of accessing phases that are unstable at larger size scales.[11]

Here, we take advantage of a reliable colloidal synthetic method, recently proposed for nanocrystals (NCs) of the orthorhombic BiSX phase (with X = Cl, Br, and I),[12] to prepare Bi sulfohalide NCs of a hexagonal phase. We reexamine, at the nanoscale, the crystallographic and electronic structure of this material, which faces controversial attribution on its stoichiometry ($Bi_{13}S_{18}X_2$ vs $Bi_{12.67}S_{18}X_2$) and displays an anomalously low band gap. We propose a solution to such a controversy by exposing the mixed valence character of Bi in the hexagonal sulfohalides, shedding light on the structure–

property relationships of a class of (nano)materials that is facing a fast growing interest.

EXPERIMENTAL SECTION

Chemicals. All chemicals were of the highest purity available unless otherwise noted and were used as received. Bismuth(III) acetate ($Bi(Ac)_3$; 99.99%) was purchased from Alfa Aesar. Oleic acid (OlCOOH, technical grade, 90%), 1-octadecene (technical grade, 90%), bis(trimethylsyil)sulfide (($Me_3Si)_2S$; synthesis grade), and sodium iodide (NaI, 99.0%) were purchased from Sigma-Aldrich. 1,1,3,3-Tetramethylthiourea (98%), trimethylsilyl bromide ((Me_3Si)-Br; 97%), and chlorotrimethylsilane ((Me_3Si)Cl; 98%) were purchased from Alfa Aesar. Benzoyl bromide (BzBr; 97%) was purchased from Acros Organics. Benzoyl chloride (BzCl; ≥98%) was purchased from TCI Europe. All solvents were anhydrous and were used as received. Dichloroethylene was purchased from Merck; toluene was purchased from Sigma-Aldrich.

Synthesis. All the colloidal NCs were synthesized in three-neck flasks connected to a standard Schlenk line under oxygen- and moisture-free conditions. In a typical synthesis yielding colloidal NCs of hexagonal Bi chalcohalide, 0.3 mmol (120 mg) of $Bi(Ac)_3$ and 3 mmol (850 mg) of oleic acid were mixed in 3 g of 1-octadecene.[12] The mixture was vigorously stirred and deaerated through repeated cycles of vacuum application and purging with nitrogen at about 80 °C. The mixture was then heated to above 100 °C to dissolve $Bi(Ac)_3$ until the solution became colorless and optically transparent, suggesting the complete formation of the bismuth(III)-oleate complex(es). The solution was cooled at 80 °C and repeatedly
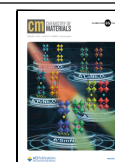
subjected to vacuum in the attempt to remove acetic acid eventually released upon the bismuth(III)-oleate complex(es) formation. The solution was then heated again under nitrogen flow, while the temperature stabilized at 180 °C. To prepare colloidal NCs of hexagonal Bi sulfobromide, half equivalent of $(Me_3Si)_2S$ (0.15 mmol, 32 μL) and half equivalent of BzBr (0.15 mmol, 18 μL) in 2 mL of octadecene were swiftly co-injected. The reaction was allowed to proceed for 15 min, then the heating mantle was removed, and the resulting colloidal dispersion was forced to quickly reach room temperature by immersion of the reaction flask in an ice bath. After the synthesis, the reaction mixture was transferred to a nitrogen-filled glove box. The crude product was centrifuged without antisolvents, the supernatant was discarded, and the resulting pellet was redispersed in anhydrous toluene and stored in a nitrogen-filled glove-box for further use. An effective tuning of the hexagonal Bi chalcohalide NC morphology was somewhat achieved by employing alternative sulfur and bromine precursors, such as tetramethylthiourea and $(Me_3Si)Br$, respectively. The syntheses of colloidal NCs of hexagonal Bi sulfoiodide were performed by using BzI as the iodine precursor; BzI was obtained by reacting BzCl with an excess (1.5 equiv) of NaI at 80 °C for 5 h. The higher reactivity of BzI compared to BzBr required the use of 0.05 mmol to obtain $Bi_{13}S_{18}I_2$ from 0.3 mmol of Bi-carboxylates (compared to 0.15 mmol of BzBr for the synthesis of $Bi_{13}S_{18}Br_2$ NCs). The syntheses of colloidal NCs of hexagonal Bi sulfochloride were attempted by using BzCl as the chloride precursor, although this phase could not be obtained. All the synthetic parameters used to obtain the colloidal NCs of hexagonal Bi sulfohalide are listed in the Supporting Information (Tables S1 and S2).

Morphological, Compositional, and Structural Characterization. Transmission electron microscopy (TEM) was used to obtain information on the NC morphology from dried colloidal dispersion and in solids thereof. Conventional TEM images were recorded with a JEOL JEM 1011 microscope, operating at an accelerating voltage of 100 kV. Samples for analysis were prepared by dropping from an NC dispersion onto Cu grids with a carbon support film and then allowing the solvent to evaporate in a vapor-controlled environment. Longitudinal and lateral sizes were determined by the statistical analysis of TEM images of several hundreds of NCs with the ImageJ software. Further, electron microscopy was carried out on a double-corrected ThermoFisher Spectra 300 S/TEM operated at 300 kV. HRTEM images were acquired using an image corrector with a parallel illumination, with the micrographs being recorded on a CMOS-based Ceta camera. HRSTEM was carried out at a convergence angle of 24 mrad with a beam current of 150 pA, recording the high-angle annular dark field (HAADF) signal. The analytical signal (energy-dispersed X-ray spectroscopy, EDX) was collected in STEM mode using a Dual-X detector and currents in the range of 0.2−1 nA.

X-ray diffraction (XRD) was used to probe the crystal structure of the NCs. Powder XRD (XPD) patterns were acquired on a lab-grade Panalytical Empyrean diffractometer operating in a parallel beam geometry and equipped with a 1.8 kW Cu Kα ceramic X-ray (45 kW), 1 mm wide incident and receiving slits, and a 40 mA PIXcel3D 2 × 2 area detector. Samples were prepared for the analysis by precipitating the NCs with ethyl acetate, discarding the supernatant and drying the precipitate under a nitrogen flux. The resulting powder was grinded in a mortar to minimize preferential orientation effects and then deposited on a zero-diffraction silicon sample holder for the analysis. Synchrotron light was used for the structural characterization of the colloidal NCs. The X-ray data were collected in two beamtime sessions at the 28ID-2 beamline of the National Synchrotron Light Source (NSLS-II) of the Brookhaven National Laboratory. The beamline was equipped with a Perkin Elmer XRD 1621 digital imaging detector having 2048 × 2048 pixels with 200 × 200 μm pixel size. The $Bi_{13}S_{18}Br_2$ NC powder samples were put in a capillary of 1 mm diameter that was spun during measurements. Measurements were performed with a beam energy of 66.18 keV (0.1874 Å), and the detector was mounted in two positions optimized for pair distribution function (PDF) and XPD data collections, i.e., respectively, 227 and

1368 mm downstream from the samples. Nickel was measured as a standard material to calibrate the wavelength and the detector geometry, including the sample-to-detector distance. Empty capillaries similar to those used for holding the NC samples were measured for background estimation. Diffraction images were azimuthally integrated and converted into intensity profiles versus 2ϑ and versus momentum transfer, $Q = 4\pi \sin \vartheta/\lambda$, by using the FIT2D program.[13] The PDF profile was calculated up to interatomic distances r of 50 Å from the Q profile by the program PDFGetX3.[14] The s maximum value of Q for PDF calculation was set to 20.0 Å^{-1} to avoid large termination effects while preserving the signal-to-noise ratio. The synchrotron XPD profile was used to identify the crystal phases among the known single-phase diffraction patterns by inquiring the POW_COD[15] (built form COD)[16] and PDF-2.0[17,18] databases via the qualitative phase analysis softwares QUALX2.0[15] and Highscore.[19] For the $Bi_{13}S_{18}Br_2$ NCs, the two most plausible candidate entries of the POW_COD database were found: no. 00-400-2831 ($Bi_{13}S_{18}I_2$, space group $P3$, ICSD code no. 243730) and no. 00-210-6883 ($Bi_{12.67}S_{18}Br_2$, space group $P6_3$, ICSD code no. 378). The CIF file of the former entry was modified by relabeling the original iodine atoms as bromine and used as a reference candidate model, with the aim of verifying if $Bi_{13}S_{18}Br_2$ is equivalent to $Bi_{12.67}S_{18}Br_2$ in describing the XPD patterns. The structural models were refined against the PDF and XPD profile by using the programs PDFGUI[20] and Fullprof,[21] respectively. In both cases, the crystal symmetry was applied to constrain lattice, displacement, and atomic position parameters. The sequential use of direct (PDF) and reciprocal (XPD) space refinements was carried out to avoid overfitting and being entrapped in local minima of the χ^2 function used in least-squares procedures. It is worth noting that PDF and XPD profiles used in this analysis are not directly related by a Fourier transform operation since the experimental setup was optimized for the two measurements. Within this approach, the optimized complementary information from a direct and reciprocal space was used to drive a more efficient structural refinement. PDF refinement was executed for interatomic distances above 1.5 Å, to avoid finite-size artifacts in the low r range, and up to 40 Å, with a step of 0.005 Å. As a first step, the scale factor, lattice parameters, peak shape parameters Q_{broad} (peak broadening from increased intensity noise at high Q), and delta1 (coefficient for $1/r$ contribution to the peak sharpening) parameters were refined separately, i.e., by keeping constant all the other parameters. As a second step, anisotropic atomic displacement parameters were included in the refinement and then the atomic position parameters were refined in the last step. More elaborated refinements were carried out by using scripts developed within the DiffPy-CMI framework,[22] which implements procedures able to refine a model consisting of a sum of two crystal phases or to account for the shape of the NCs. These have been used to address the ambiguity between $Bi_{12.67}S_{18}Br_2$ and $Bi_{13}S_{18}Br_2$ structural models. XPD refinement was carried out by the Rietveld method.[23] Fitting parameters were the scale factor parameters, profile parameters, i.e., full width at half-maximum (FWHM) and peak asymmetry, and unit cell parameters. In particular, the FWHM was described by spherical harmonics parameters, and the final value allowed us to extract the crystallite shape.[24] The background was interpolated and not refined. The refinement parameters of PDF and XPD profiles are reported in Tables S3 and S4, respectively. The program RootProf was used to convert the XPD profiles in the CuK$_{\alpha 1}$ wavelength.[25]

Optical Characterization. The optical properties of the $Bi_{13}S_{18}X_2$ NCs were investigated on both colloidal dispersions and thin films (prepared by spin casting NC dispersions on glass substrates). A PerkinElmer UV–vis–NIR spectrophotometer (Lambda 1050) was used to measure the transmission and reflectance spectra of the NCs in the 300−1600 nm range; a 150 mm InGaAs integration sphere was used to acquire reflectance spectra. The optical band gap values of the NCs were estimated by Tauc analysis.[26,27] A Dektak contact profilometer (D150 Veeco) was used to determine the thickness of the casted NC films and, therefore, to estimate the NC absorption coefficients. The reflectance (R) of the NC thin films was determined with an integrating sphere; the measurement of the transmittance (T)

allowed us to estimate the absorptance (A, with $1 = A + T + R$) of the NCs. Upon measuring the thickness (d) of the thin films, we estimated the NC absorption coefficient (α) by using the Lambert–Beer law ($I = I_0 e^{-\alpha d}$, in which $I_0 = 1 - R$ is the light incident on the NC films and $I = T$ is the light transmitted by the NC films).

Theoretical Calculations. Density functional theory (DFT) simulations were run to infer the electronic band structure of the Bi chalcohalide NCs. The calculations were run through the VASP code[28] within the plane-augmented wave framework.[29] The Perdew–Burke–Ernzerhof (PBE) functional[30] was adopted throughout and complemented with the Tkatchenko–Scheffler correction[31] to accurately reproduce dispersive forces. When not otherwise specified, the following settings were adopted. The plane-wave energy cutoff was set to 500 eV for geometry optimizations and 400 eV for band structure calculations. The reciprocal space was sampled through a uniform, Γ-centered grid with $0.28/2\pi$ Å^{-1} point spacing. For all the studied systems, the cell parameters and atomic positions were optimized to the closest energy minimum. Both the geometry optimization and self-consistent procedures were stopped when the energy difference between two consecutive steps was lower than 10^{-6} eV. Structures and isosurfaces were drawn with the VESTA software.[32] Spin–orbit coupling (SOC) was not included in the simulations presented in the main text. Our previous work[12] on similar compounds showed that SOC has a negligible effect on geometries and energy differences. Concerning the band gaps, the neglection of SOC and the adoption of generalized gradient approximation (GGA) functionals such as PBE are known to lead to an error compensation resulting in qualitatively accurate results. We performed test simulations on $Bi_{13}S_{18}Br_2$ and noted that the only significant change is the length of the Bi–Bi dimer, which elongates (from 3.158 to 3.215 Å). This finding is in line with the proposed p^1-like configuration of the Bi atoms forming the dimers, an electronic configuration whose electronic energy levels are known to undergo electronic energy splitting due to SOC, thereby affecting bond lengths and energies. Nonetheless, the nature of valence and conduction bands in $Bi_{13}S_{18}X_2$ (X = Br and I) is not affected by the neglection of SOC, as shown in Figure S21.

RESULTS AND DISCUSSION

Our synthetic approach involves the hot co-injection of both the S and X (= Cl, Br, and I) precursors to a solution of Bi-carboxylate complexes. Such an approach allows tuning of the Bi:S:X stoichiometric ratio by independently controlling the corresponding precursor concentration, permitting to explore the Bi-S-X ternary phase diagram.[12] Compared to heat-up approaches,[33] our method granted direct access to the chosen reaction temperature (180 °C), preventing the formation of the undesired Bi_2S_3 phase (Figure S1). Another advantage of our method compared to previous reports is that it does not yield powders, which would demand for a polymer-assisted processing to disperse the NCs,[34] nor it requires almost stoichiometric amounts of Al^{3+} cations to prevent the formation of Bi_2S_3.[35]

Compared to our previous work, in which we obtained phase pure orthorhombic BiSX NCs,[12] an increased S:X molar ratio permitted us to prepare phase pure hexagonal Bi chalcohalide NCs. In the particular case of the Bi sulfobromides, when the molar ratio of the co-injected precursors was S:Br = 1:1, a darkish dispersion formed (Figure 1a). This is strikingly different from the reddish dispersion of orthorhombic BiSBr NCs obtained with S:Br = 1:2.[12] TEM inspection showed rod-like NCs (Figure 1b and Figure S2), 100 nm long and 20 nm wide (both with a ~15% polydispersity; Figure S3). High-resolution TEM revealed a high degree of crystallinity for all the NCs (Figure 1c–e), regardless of their morphological differences. Observed in
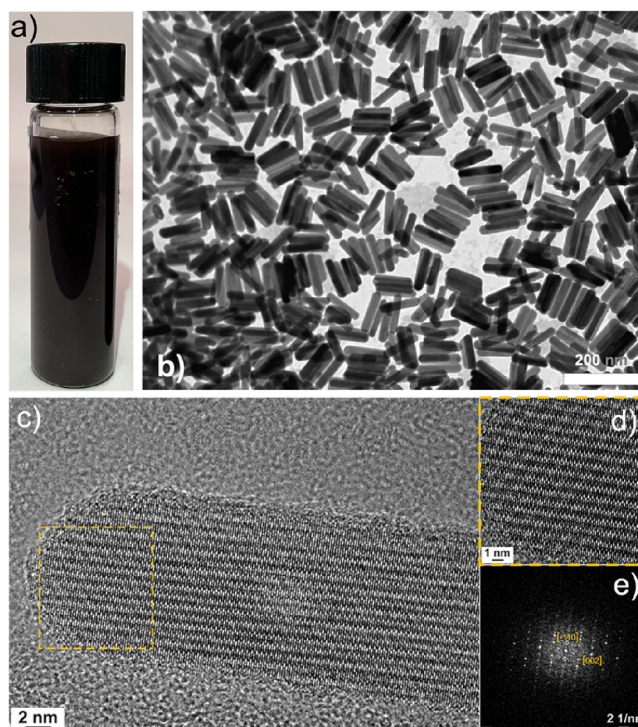

Figure 1. (a) Day-light picture of a toluene colloidal dispersion of the hexagonal Bi sulfobromide NCs; (b) TEM micrograph of the NCs; (c) HRTEM of an NC portion, (d) high magnification view, and (e) its fast Fourier transform.

HAADF-STEM, the NCs often displayed an irregular contrast, suggesting a rough surface or the presence of cavities (Figure S4). Nevertheless, the composition was found to be homogeneous from EDX analysis (Figure S5). Since oleic acid is the only amphiphilic molecule in our synthetic protocol,[12] we expect that such species coordinate the surface of our NCs, thus exposing oleyl pendant moieties to the surroundings.

XPD revealed a unique hexagonal phase in the NC sample (vide infra). It corresponds to a compound that was previously identified as $Bi_{12.67}S_{18}Br_2$ (or $Bi_{19}S_{27}Br_3$),[36] until a subsequent reexamination suggested that it could be described as $Bi_{13}S_{18}Br_2$ (isostructural to the $Bi_{13}S_{18}I_2$ reported in the study examining this issue).[37] These two structures are almost identical, being both constituted by Bi–S networks that can be described as the structure of Bi_2S_3 rolling up to form hexagonal and triangular channels parallel to the c axis and occupied by columns of Bi and Br atoms, respectively. The only difference lies in such columns of Bi atoms (highlighted in red in Figure 2a and hereafter referred to as columnar Bi), which are formed by non-interacting Bi atoms in $Bi_{12.67}S_{18}Br_2$ or by Bi dimers in $Bi_{13}S_{18}Br_2$ (Figure 2b and Figure S6).

The NC size could be tuned by employing S and Br precursors with different reactivities, such as combinations of bis(trimethylsilyl)sulfide (($Me_3Si)_2S$) or 1,1,3,3-tetramethylthiourea and benzoyl bromide (BzBr) or ($Me_3Si)Br$, with less reactive precursors yielding NCs with a higher aspect ratio (Figures S7 and S8), likely due to a preferential accretion along the c axis consistently with the highly anisotropic structure and in analogy to previous observations for orthorhombic BiSBr NCs.[12] Similarly, we expect to exert further control on the NC size and shape by using libraries of Bi-complexes as reagents.[9] In addition, the use of I precursors, such as BzI, allowed us to
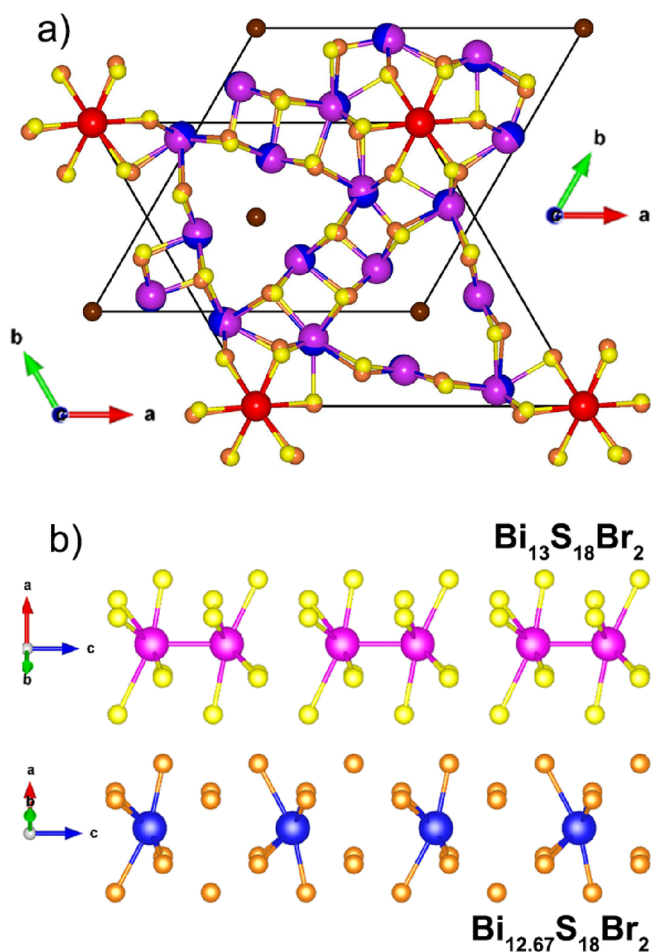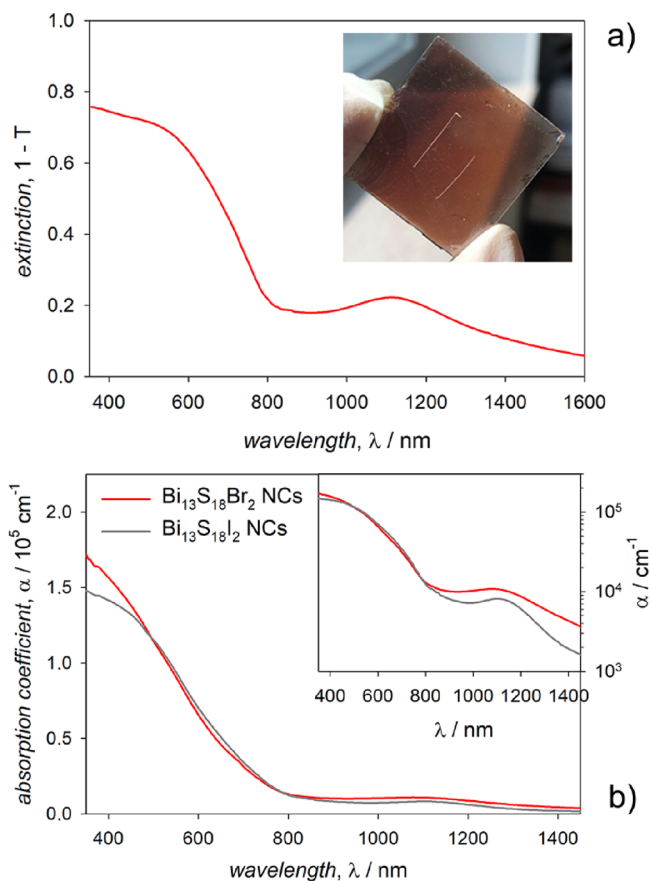
Figure 2. (a) Superimposed models of $Bi_{13}S_{18}Br_2$ (pink Bi and yellow S) and $Bi_{12.67}S_{18}Br_2$ (blue Bi and orange S) and (b) details on the S coordination of the columnar Bi atoms (which are highlighted in red in the superimposed structures).


Figure 3. (a) Extinction spectrum of the hexagonal Bi sulfobromide NC thin film and (b) absorption coefficients of hexagonal Bi sulfohalide NC thin films (plotted in the $\log_{10}$ scale in the inset).

prepare phase pure hexagonal Bi sulfoiodide NCs (Figures S9 and S10), whereas the use of Cl precursors, such as BzCl or (Me₃Si)Cl, only yielded orthorhombic BiSCl NCs (data not shown).[12]

The extinction spectrum (i.e., both absorption and scattering of the incident light) of the hexagonal Bi sulfohalide NCs showed a broad peak in the NIR spectral region and a more intense feature in the vis spectral range (Figure 3). Remarkably, such a NIR absorption band was previously reported for both the $Bi_{13}S_{18}Br_2$ and the $Bi_{12.67}S_{18}Br_2$ structures.[34,35] We determined the absorption coefficient of the hexagonal Bi sulfohalide NCs, yielding values on the order of 10^4 cm^{-1} for the broad band centered at about 1100 nm (Figure 3b), with a negligible dependence on the halogen (Br or I). We estimated for the hexagonal Bi sulfohalide NCs indirect band gaps of about 0.80 eV (Figures S11 and S12), which are well below those of the orthorhombic BiSX NCs (ranging between 2.1 and 1.5 eV; with lower values, the heavier the X element; Figure S13);[12] oddly, the hexagonal Bi sulfohalide NCs showed band gap values fairly narrower than that of Bi_2S_3 (which is ~1.3 eV),[38] despite the small halogen contribution to the overall composition.

The origin of such an unexpectedly low band gap was investigated by DFT simulations on both the $Bi_{13}S_{18}Br_2$ and $Bi_{12.67}S_{18}Br_2$ models. $Bi_{13}S_{18}Br_2$ displays an isolated, occupied

band in the middle of the band gap (Figure 4a). The corresponding charge density and DOS orbital projections identified this band as a localized p−p sigma bond between pairs of subvalent, columnar Bi atoms (Figure 4a). This represents the electronic origin of the formation of the dimers, which are formally Bi_2^{4+} entities.[37] The bottom of the conduction band is localized on the Bi^{3+} atoms of the main Bi−S framework, with a contribution of the surrounding S atoms, whereas the Bi_2^{4+} dimer antibonding states lie at higher energies (Figure S14). The small overlap between the valence and conduction bands entails a weak intensity for the corresponding optical transition (0.72 eV), which can thus be assigned to the experimental NIR absorption peak (Figure 3a). This transition can be regarded as an intervalence charge transfer, being related to the mixed valence character of $Bi_{13}S_{18}X_2$ and involving the occupied σ orbitals of the Bi_2^{4+} dimers and the empty 6p orbitals of Bi^{3+} in the main Bi−S framework. Notably, the band gap of $Bi_{13}S_{18}Br_2$ calculated excluding the dimer state is similar to that of the $Bi_{12.67}S_{18}Br_2$ structure (1.55 and 1.39 eV, respectively; Figure 4).

The formation of the Bi_2^{4+} dimer can be considered as resulting from Peierls distortions. The $Bi_{13}S_{18}Br_2$ structure features an extra valence electron per unit formula compared to $Bi_{12.67}S_{18}Br_2$. In $Bi_{13}S_{18}Br_2$, each extra electron occupies one of the $6p_z$ orbitals localized on the columnar Bi cations (which constitute the bottom of the conduction band in the $Bi_{12.67}S_{18}Br_2$ structure), thus formally becoming Bi^{2+}. As the Bi^{3+} cations can be considered as closed shell species (since their 6s orbitals lie more than 8 eV below the Fermi level;
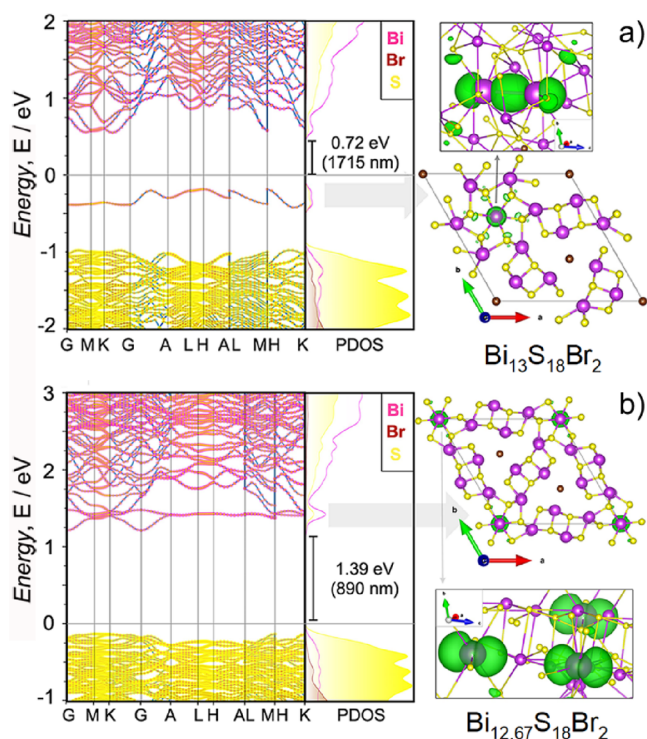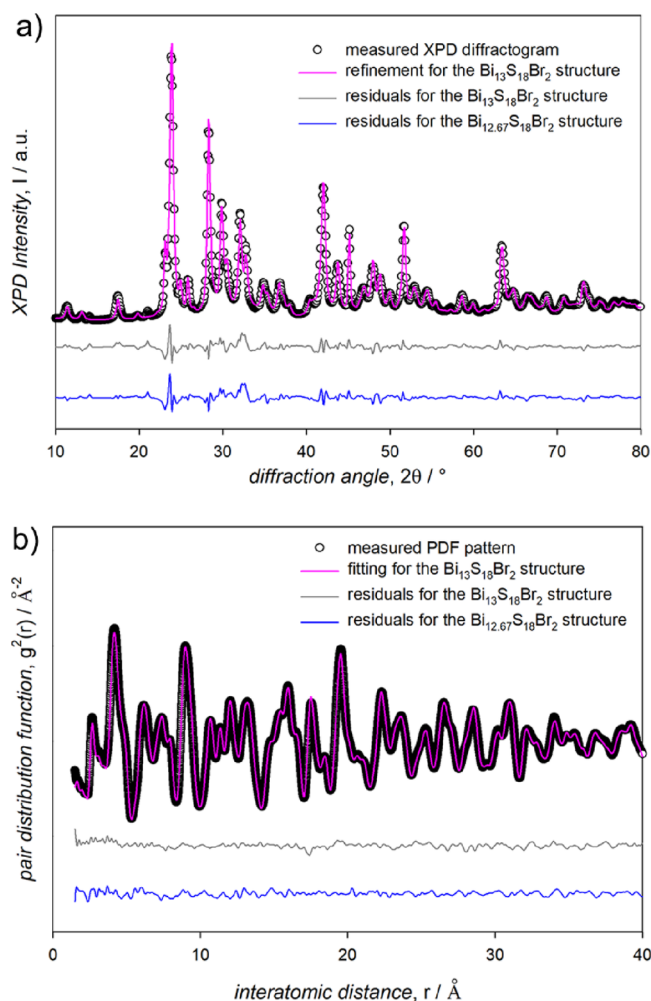
Figure 4. Band structure, density of states (DOS), and partial charge density for (a) $Bi_{13}S_{18}Br_2$ and (b) $Bi_{12.67}S_{18}Br_2$. Partial charge densities (green isosurfaces) were calculated from the electronic states within the energy ranges: $-0.5/0.0$ eV (a) and $+1.0/+1.7$ eV (b).

Figure 5. (a) Rietveld fit of the XPD data with the $Bi_{13}S_{18}Br_2$ model and residuals of the fitting procedure for both the $Bi_{13}S_{18}Br_2$ and $Bi_{12.67}S_{18}Br_2$ structures (to facilitate the comparison with data collected on lab-grade setups, the 2θ values of the XPD horizontal axis were converted to emulate the $CuK\alpha_1$ radiation). (b) Fitting of the PDF data with the $Bi_{13}S_{18}Br_2$ model and residuals of the fitting procedure for both the $Bi_{13}S_{18}Br_2$ and $Bi_{12.67}S_{18}Br_2$ structures.

Figure S14), $Bi_{13}S_{18}Br_2$ displays one valence electron per columnar Bi atom. This represents the typical scenario in which dimers are expected to form due to Peierls distortions.[39,40] This scenario is confirmed by the metallic character of $Bi_{13}S_{18}Br_2$ that results when simulating equidistance between the subvalent columnar Bi atoms (Figure S15). Indeed, Peierls transitions imply that the formation of dimers opens a gap. The lower energy associated to the formation of a doubly occupied, low-lying $Bi^{2+}-Bi^{2+}$ bonding state and an empty antibonding state compensates the destabilization induced by the presence of subvalent Bi^{2+} cations.

In the attempt to confirm that the $Bi_{13}S_{18}X_2$ model is adequate to describe the structure of our NCs, we relied on synchrotron XPD and PDF data (Figure 5).

The need of describing the dimers resulted in a formal reduction of the crystal structure symmetry from the hexagonal $P6_3$ to the trigonal $P3$ space group, albeit the main Bi–S frame complies with all the symmetry operations of the $P6_3$ space group. The Rietveld refinement of XPD data yielded comparably good fits for both $Bi_{13}S_{18}Br_2$ and $Bi_{12.67}S_{18}Br_2$ structures (Figure 5a and Figure S16). The refinement of the anisotropic crystallite shape confirmed that the NCs are elongated along their c axis (Figure S17). Analogously, the refinement of the PDF profiles produced comparable results for both the $Bi_{13}S_{18}Br_2$ and the $Bi_{12.67}S_{18}Br_2$ structures (Figure 5b and Figure S18). We note that the predominant effects of the crystallite morphology, i.e., the nanoscopic size and the highly anisotropic shape, may conceal the impact that the small differences between the two models (a Bi cation every 98 atoms) can have on the diffraction data.

We also adopted DFT calculations to estimate the distribution of Bi atoms among the partially occupied crystallographic sites of $Bi_{13}S_{18}Br_2$ and $Bi_{12.67}S_{18}Br_2$ structures. In the $Bi_{13}S_{18}Br_2$, the Bi^{2+} cations stabilized at a bonding distance ($d_{Bi-Bi} = 3.16$ Å) compatible with the formation of a dimer (Figure S19);[37] conversely, for the $Bi_{12.67}S_{18}Br_2$, the most stable configuration maximizes the Bi–Bi distance ($d_{Bi-Bi} = 6.03$ Å; Figure S20). For both structures, however, we observed several degenerate Bi configurations that lie close to the lowest energy, in agreement with the observed positional disorder of the columnar Bi atoms. Despite our extended analysis, we could not unambiguously attribute one of the two structures to the as-synthesized NCs; therefore, we cannot definitely exclude that $Bi_{13}S_{18}X_2$ and $Bi_{12.67}S_{18}X_2$ may coexist. Nevertheless, we note that the $Bi_{13}S_{18}X_2$ structure guarantees a complete coordination of the S atoms that delimitate the hexagonal channels in which the columnar Bi atoms are located, whereas some of such S atoms are undercoordinated in the $Bi_{12.67}S_{18}X_2$ model (Figure 2b). Moreover, the anomalously low band gap of our NCs can be unequivocally attributed to the $Bi_{13}S_{18}Br_2$ structure only, as inferred from

first-principle calculations. On this basis, we suggest that the as-synthesized, hexagonal Bi sulfohalide NCs adopt mainly, if not exclusively, the $Bi_{13}S_{18}X_2$ structure.

CONCLUSIONS

We remark the versatility of our colloidal synthetic method to prepare phase-pure Bi chalcohalide NCs.[12] We propose that the here presented hexagonal Bi chalcohalide NCs adopt the $Bi_{13}S_{18}X_2$ structure showing a mixed valence character, which arises from Bi atoms displaying two different oxidation states in distinct crystallographic sites. This gives rise to an intervalence charge transfer absorption band in the NIR spectral region that accounts for its narrow band gap, uncommon for binary and ternary compounds with Bi-chalcogen−halogen composition. This represents a fundamental contribution to uncover the structure−property relationships of a material that is facing a rising interest and is being employed for diverse applications, ranging from photovoltaics[41,42] and photocatalysis[43,44] to thermoelectrics.[34,45] This work thus expands our knowledge on the chemistry, structure, and properties of metal chalcohalide nanomaterials and contributes to establish this class of mixed anion semiconductors as an effective complement to metal chalcogenides and metal halides.

ASSOCIATED CONTENT

Ⓢ Supporting Information

The Supporting Information is available free of charge at https://pubs.acs.org/doi/10.1021/acs.chemmater.2c02941.

> Synthetic parameters, structural refinement parameters, structural, morphological, and compositional characterization, optical properties, and electronic structure calculations (PDF)
>
> Crystallographic data for $Bi_{13}S_{18}I_2$, space group $P3$ (CIF)
>
> Another crystallographic data for $Bi_{13}S_{18}I_2$, space group $P3$ (CIF)
>
> Crystallographic data for $Bi_{12.67}S_{18}Br_2$, space group $P6_3$ (CIF)

AUTHOR INFORMATION

Corresponding Authors

Gabriele Saleh − *Istituto Italiano di Tecnologia − IIT, 16163 Genova, Italy;* ⓘ orcid.org/0000-0002-6201-9546; Email: gabrielesaleh@outlook.com

Rocco Caliandro − *Consiglio Nazionale delle Ricerche, Istituto di Cristallografia − CNR IC, 70126 Bari, Italy;* ⓘ orcid.org/0000-0002-0368-4925; Email: rocco.caliandro@ic.cnr.it

Carlo Giansante − *Consiglio Nazionale delle Ricerche, Istituto di Nanotecnologia − CNR NANOTEC, 73100 Lecce, Italy;* ⓘ orcid.org/0000-0003-4558-5367; Email: carlo.giansante@nanotec.cnr.it

Authors

Danila Quarta − *Consiglio Nazionale delle Ricerche, Istituto di Nanotecnologia − CNR NANOTEC, 73100 Lecce, Italy*

Stefano Toso − *Istituto Italiano di Tecnologia − IIT, 16163 Genova, Italy; International Doctoral Program in Science, Università Cattolica del Sacro Cuore, 25121 Brescia, Italy;* ⓘ orcid.org/0000-0002-1621-5888

Anna Moliterni − *Consiglio Nazionale delle Ricerche, Istituto di Cristallografia − CNR IC, 70126 Bari, Italy*

Andrea Griesi − *Istituto Italiano di Tecnologia − IIT, 16163 Genova, Italy*

Giorgio Divitini − *Istituto Italiano di Tecnologia − IIT, 16163 Genova, Italy;* ⓘ orcid.org/0000-0003-2775-610X

Ivan Infante − *Istituto Italiano di Tecnologia − IIT, 16163 Genova, Italy; BCMaterials, Basque Center for Materials, Applications, and Nanostructures, UPV/EHU Science Park, Leioa 48940, Spain; Ikerbasque, Basque Foundation for Science, Bilbao 48009, Spain;* ⓘ orcid.org/0000-0003-3467-9376

Giuseppe Gigli − *Consiglio Nazionale delle Ricerche, Istituto di Nanotecnologia − CNR NANOTEC, 73100 Lecce, Italy; Dipartimento di Fisica, Università del Salento, 73100 Lecce, Italy*

Cinzia Giannini − *Consiglio Nazionale delle Ricerche, Istituto di Cristallografia − CNR IC, 70126 Bari, Italy;* ⓘ orcid.org/0000-0003-0983-2885

Liberato Manna − *Istituto Italiano di Tecnologia − IIT, 16163 Genova, Italy;* ⓘ orcid.org/0000-0003-4386-7985

Complete contact information is available at:
https://pubs.acs.org/10.1021/acs.chemmater.2c02941

Author Contributions

○D.Q. and S.T. contributed equally.

Author Contributions

All authors have given approval to the final version of the manuscript.

Notes

The authors declare the following competing financial interest(s): I declare the potentially competing interests of some of the authors (C. Gians., D. Q., S. T., R. C., A. M., C. Giann., L. M., G. G.) as co-inventors on a provisional patent application entitled Process for the Production of Nanocrystals of Metal Chalcohalides, IT 102022000001577.

REFERENCES

(1) Day, P.; Hush, N. S.; Clark, R. J. H. Mixed Valence: Origins and Developments. *Philos. Trans. R. Soc., A* **2008**, *366*, 5−14.

(2) Robin, M. B. The Color and Electronic Configurations of Prussian Blue. *Inorg. Chem.* **1962**, *1*, 337−342.

(3) Herrera, J. M.; Bachschmidt, A.; Villain, F.; Bleuzen, A.; Marvaud, V.; Wernsdorfer, W.; Verdaguer, M. Mixed valency and

magnetism in cyanometallates and Prussian blue analogues. *Philos. Trans. R. Soc., A* **2008**, *366*, 127−138.

(4) Cava, R. J.; Batlogg, B.; Krajewski, J. J.; Farrow, R.; Rupp, L. W.; White, A. E., Jr.; Short, K.; Peck, W. F.; Kometani, T. Super-conductivity near 30 K without copper: the $Ba_{0.6}K_{0.4}BiO_3$ perovskite. *Nature* **1988**, *332*, 814−816.

(5) Raveau, B. The crucial role of mixed valence in the magnetoresistance properties of manganites and cobaltites. *Philos. Trans. R. Soc., A* **2008**, *366*, 83−92.

(6) Day, P. Spectra and Constitution of Antimony(III) Antimony-(V) Hexahalide Salts and Related Compounds. *Inorg. Chem.* **1963**, *2*, 452−456.

(7) Mohanta, S. K.; Mishra, S. N.; Iyer, K. K.; Sampathkumaran, E. V. Microscopic evidence for 4f localization with reduced particle size in correlated electron system $CePd_3$. *Phys. Rev. B* **2013**, *87*, No. 125125.

(8) Zhang, L. L.-M.; Zhou, G.; Zhou, G.; Lee, H. K.; Zhao, N.; Prezhdo, O. V.; Mak, T. C. W. Core-dependent properties of copper nanoclusters: valence-pure nanoclusters as NIR TADF emitters and mixed-valence ones as semiconductors. *Chem. Sci.* **2019**, *10*, 10122−10128.

(9) Giansante, C. Library Design of Ligands at the Surface of Colloidal Nanocrystals. *Acc. Chem. Res.* **2020**, *53*, 1458.

(10) Nai, J.; Wang, S.; Lou, X. W. Ordered colloidal clusters constructed by nanocrystals with valence for efficient CO_2 photo-reduction. *Sci. Adv.* **2019**, *5*, No. eaax5095.

(11) Tappan, B. A.; Brutchey, R. L. Polymorphic Metastability in Colloidal Semiconductor Nanocrystals. *ChemNanoMat* **2020**, *6*, 1567.

(12) Quarta, D.; Toso, S.; Giannuzzi, R.; Caliandro, R.; Moliterni, A.; Saleh, G.; Capodilupo, A.-L.; Debellis, D.; Prato, M.; Nobile, C.; Maiorano, V.; Infante, I.; Gigli, G.; Giannini, C.; Manna, L.; Giansante, C. Colloidal Bismuth Chalcohalide Nanocrystals. *Angew. Chem., Int. Ed.* **2022**, *134*, No. e202201747.

(13) Hammersley, A. P.; Svensson, S. O.; Hanfland, M.; Fitch, A. N.; Hauserman, D. Two-dimensional detector software: From real detector to idealised image or two-theta scan. *High Press. Res.* **1996**, *14*, 235−248.

(14) Juhás, P.; Davis, T.; Farrow, C. L.; Billinge, S. J. L. PDFgetX3: a rapid and highly automatable program for processing powder diffraction data into total scattering pair distribution functions. *J. Appl. Crystallogr.* **2013**, *46*, 560−566.

(15) Altomare, A.; Corriero, N.; Cuocci, C.; Falcicchio, A.; Moliterni, A.; Rizzi, R. QUALX2. 0: a qualitative phase analysis software using the freely available database POW_COD. *J. Appl. Crystallogr.* **2015**, *48*, 598−603.

(16) Gražulis, S.; Daškevič, A.; Merkys, A.; Chateigner, D.; Lutterotti, L.; Quirós, M.; Serebryanaya, N. R.; Moeck, P.; Downs, R. T.; Le Bail, A. Crystallography Open Database (COD): an open-access collection of crystal structures and platform for world-wide collaboration. *Nucleid Acids Res.* **2012**, *40*, D420−D427.

(17) Faber, J.; Fawcett, T. The powder diffraction file: present and future. *Acta Cryst. B* **2002**, *58*, 325.

(18) Kabekkodu, S. N.; Faber, J.; Fawcett, T. New Powder Diffraction File (PDF-4) in relational database format: advantages and data-mining capabilities. *Acta Cryst. B* **2002**, *58*, 333.

(19) Degen, T.; Sadki, M.; Bron, E.; König, U.; Nénert, G. The HighScore suite. *Powder Diffr.* **2014**, *29*, S13.

(20) Farrow, C. L.; Juhás, P.; Liu, J. W.; Bryndin, D.; Božin, E. S.; Bloch, J.; Proffen, T.; Billinge, S. J. L. PDFfit2 and PDFgui: computer programs for studying nanostructure in crystals. *J. Phys.: Condens. Matter* **2007**, *19*, No. 335219.

(21) Rodríguez-Carvajal, J. Recent advances in magnetic structure determination by neutron powder diffraction. *Phys. B* **1993**, *192*, 55.

(22) Juhás, P.; Farrow, C. L.; Yang, X.; Knox, K. R.; Billinge, S. J. L. Complex modeling: a strategy and software program for combining multiple information sources to solve ill posed structure and nanostructure inverse problems. *Acta Cryst. A* **2015**, *71*, 562.

(23) Rietveld, H. M. A profile refinement method for nuclear and magnetic structures. *J. Appl. Crystallogr.* **1969**, *2*, 65.

(24) McCusker, L. B.; Von Dreele, R. B.; Cox, D. E.; Louer, D.; Scardi, P. Rietveld refinement guidelines. *J. Appl. Crystallogr.* **1999**, *32*, 36.

(25) Caliandro, R.; Belviso, D. B. RootProf: software for multivariate analysis of unidimensional profiles. *J. Appl. Crystallogr.* **2014**, *47*, 1087.

(26) Tauc, J.; Grigorovici, R.; Vancu, A. Optical Properties And Electronic Structure of Amorphous Germanium. *Phys. Status Solidi B* **1966**, *15*, 627.

(27) Davis, E. A.; Mott, N. F. Conduction in non-crystalline systems V. Conductivity, optical absorption and photoconductivity in amorphous semiconductors. *Philos. Mag.* **1970**, *22*, No. 0903.

(28) Kresse, G.; Furthmüller, J. Efficiency of ab-initio total energy calculations for metals and semiconductors using a plane-wave basis set. *Comput. Mater. Sci.* **1996**, *6*, 15.

(29) Blöchl, P. E. Projector augmented-wave method. *Phys. Rev. B* **1994**, *50*, 17953.

(30) Perdew, J. P.; Burke, K.; Ernzerhof, M. Generalized Gradient Approximation Made Simple. *Phys. Rev. Lett.* **1996**, *77*, 3865.

(31) Tkatchenko, A.; Scheffler, M. Accurate Molecular Van Der Waals Interactions from Ground-State Electron Density and Free-Atom Reference Data. *Phys. Rev. Lett.* **2009**, *102*, No. 073005.

(32) Momma, K.; Izumi, F. VESTA 3 for three-dimensional visualization of crystal, volumetric and morphology data. *J. Appl. Crystallogr.* **2011**, *44*, 1272.

(33) Toso, S.; Akkerman, Q. A.; Martín-García, B.; Prato, M.; Zito, J.; Infante, I.; Dang, Z.; Moliterni, A.; Giannini, C.; Bladt, E.; Lobato, I.; Ramade, J.; Bals, S.; Buha, J.; Spirito, D.; Mugnaioli, E.; Gemmi, M.; Manna, L. Nanocrystals of Lead Chalcohalides: A Series of Kinetically Trapped Metastable Nanostructures. *J. Am. Chem. Soc.* **2020**, *142*, 10198.

(34) Xu, B.; Feng, T.; Agne, M. T.; Tan, Q.; Li, Z.; Imasato, K.; Zhou, L.; Bahk, J.-H.; Ruan, X.; Snyder, G. J.; Wu, Y. Manipulating Band Structure through Reconstruction of Binary Metal Sulfide for High-Performance Thermoelectrics in Solution-Synthesized Nano-structured $Bi_{13}S_{18}I_2$. *Angew. Chem., Int. Ed.* **2018**, *57*, 2413−2418.

(35) Wu, Y.; Pan, H.; Zhou, X.; Li, M.; Zhou, B.; Yang, C.; Zhang, W.-H.; Jie, J.; Li, C. Shape and composition control of $Bi_{19}S_{27}(Br_{3−x}I_x)$ alloyed nanowires: the role of metal ions. *Chem. Sci.* **2015**, *6*, 4615−4622.

(36) Mariolacos, K. The crystal structure of $Bi(Bi_2S_3)_9Br_3$. *Acta Cryst. B* **1976**, *32*, 1947.

(37) Groom, R.; Jacobs, A.; Cepeda, M.; Drummey, R.; Latturner, S. E. $Bi_{13}S_{18}I_2$: (Re)discovery of a Subvalent Bismuth Compound Featuring $[Bi_2]^{4+}$ Dimers Grown in Sulfur/Iodine Flux Mixtures. *Chem. Mater.* **2017**, *29*, 3314−3323.

(38) Cao, Y.; Bernechea, M.; Maclachlan, A.; Zardetto, V.; Creatore, M.; Haque, S. A.; Konstantatos, G. Solution Processed Bismuth Sulfide Nanowire Array Core/Silver Sulfide Shell Solar Cells. *Chem. Mater.* **2015**, *27*, 3700.

(39) Peierls, R. E. *Quantum Theory of Solids*; Oxford University Press: London, 1955.

(40) Fincher, C. R.; Chen, C. E.; Heeger, A. J.; MacDiarmid, A. G.; Hastings, J. B. *Phys. Rev. Lett.* **1982**, *48*, 100.

(41) Palazon, F. Metal Chalcohalides: Next Generation Photovoltaic Materials? *Solar RRL* **2022**, *6*, No. 2100829.

(42) Li, S.; Xu, L.; Kong, X.; Kusunose, T.; Tsurumachi, N.; Feng, Q. $Bi_{13}S_{18}X_2$-Based Solar Cells (X = Cl, Br, I): Photoelectric Behavior and Photovoltaic Performance. *Phys. Rev. Appl.* **2021**, *15*, No. 034040.

(43) Li, J.; Pan, W.; Liu, Q.; Chen, Z.; Chen, Z.; Feng, X.; Chen, H. Interfacial Engineering of $Bi_{19}Br_3S_{27}$ Nanowires Promotes Metallic Photocatalytic CO_2 Reduction Activity under Near-Infrared Light Irradiation. *J. Am. Chem. Soc.* **2021**, *143*, 6551.

(44) Ai, L.; Wang, L.; Xu, M.; Zhang, S.; Guo, N.; Jia, D.; Jia, L. Defective $Bi_{333}(Bi_6S_9)Br/Bi_2S_3$ heterostructure nanorods: Boosting the activity for efficient visible-light photocatalytic Cr(VI) reduction. *Appl. Catal., B* **2021**, *284*, No. 119730.

(45) Wang, Y.; Dai, X.; Dong, C.; Guo, W.; Xu, Z.; Chen, Y.; Xiang, H.; Zhang, R. Engineering Electronic Band Structure of Binary

Thermoelectric Nanocatalysts for Augmented Pyrocatalytic Tumor Nanotherapy. *Adv. Mater.* **2022**, *34*, No. 2106773.

(46) Ponti, G. et al. The role of medium size facilities in the HPC ecosystem: the case of the new CRESCO4 cluster integrated in the ENEAGRID infrastructure. *Proceedings of the 2014 International Conference on High Performance Computing and Simulation*, HPCS, 2014, *6903807*, 1030−1033.

📖 **Recommended by ACS**

Understanding and Preventing Photoluminescence Quenching to Achieve Unity Photoluminescence Quantum Yield in Yb:YLF Nanocrystals

Jence T. Mulder, Arjan J. Houtepen, *et al.*

JANUARY 06, 2023
ACS APPLIED MATERIALS & INTERFACES   READ ☑

Red−NIR Luminescence in Rare-Earth and Manganese Ions Codoped $Cs_4CdBi_2Cl_{12}$ Vacancy-Ordered Quadruple Perovskites

Peipei Dang, Jun Lin, *et al.*

FEBRUARY 07, 2023
CHEMISTRY OF MATERIALS   READ ☑

Chemically Sculpturing the Facets of $CsPbBr_3$ Perovskite Platelet Nanocrystals

Souvik Banerjee, Narayan Pradhan, *et al.*

DECEMBER 28, 2022
ACS NANO   READ ☑

Inorganic Ligand Triggered Transformation from Cs_4PbBr_6 Nanocrystals to Blue-Emitting $CsPbBr_3$ Nanoplatelets

Rui Yun, Xiyan Li, *et al.*

DECEMBER 30, 2022
CHEMISTRY OF MATERIALS   READ ☑

Get More Suggestions >